

# Initial formation of channels and shoals in a short tidal embayment

By **H. M. SCHUTTELAARS** AND **H. E. DE SWART**

Institute for Marine and Atmospheric Research, Utrecht University, P.O. Box 80.000,  
3508 TA Utrecht, The Netherlands

(Received 21 April 1997 and in revised form 7 July 1998)

It is demonstrated, by using a simple model, that bedforms in a short tidal embayment can develop due to a positive feedback between tidal currents, sediment transport and bedforms. The water motion is modelled by the depth integrated shallow water equations. The system is forced by a prescribed free-surface elevation at the entrance of the embayment. For the sediment dynamics a diffusively dominated suspended load transport model is considered. Tidal averaging is used to obtain the bottom profiles at the long morphological time scale.

The stability of a constantly sloping equilibrium bottom profile is studied for various combinations of the model parameters. It turns out that without a mechanism that generates vorticity this equilibrium profile is stable. In that case small-scale perturbations can at most become marginally stable if no bedload term in the bottom evolution equation is incorporated. If vorticity is generated, in our model by bottom friction torques, the basic state is unstable. The spatial patterns of the unstable modes and their growth rates depend, among other things, on the strength of the bottom friction, the width of the embayment and the grain size: if the sediment under consideration consists of large particles, the equilibrium will be more stable than when smaller particles are considered. Without a diffusive term in the bed evolution equation, small-scale perturbations become unstable. To avoid this physically unrealistic behaviour bedload terms are included in the sediment transport. Furthermore, it is shown that using an asymptotic expansion for the concentration as given in earlier literature is only valid for small or moderate mode numbers and the technique is extended to large mode numbers. A physical interpretation of the results is also given.

---

## 1. Introduction

In most tidal embayments a delicate balance exists between the water motion and the morphology of the domain. During the flood period large amounts of sediment are transported into the embayment, while during the ebb period most of this sediment leaves the embayment again. Owing to erosion and deposition during the tidal cycle, the bottom evolves and usually organizes itself in a pattern of shallow sandy shoals separated by deep channels, see e.g. Ehlers (1988). The channel system often exhibits a fractal-like structure with the number of channels increasing and their depth decreasing in the landward direction. Understanding the behaviour of channels and shoals is very important, from both an ecological and economic point of view. Since the sediment balance in these tidal embayments is very sensitive to external factors (McBride, Byrnes & Hiland 1995), the equilibrium in these regions can be easily disturbed. A well-studied example is the Frisian inlet and adjacent basin: in

1969 part of this system (the Lauwers Sea) was closed by a dam. This reduced the tidal prism (the embayment volume between high and low water level) of the system by 30% (Oost 1995) and its dynamic equilibrium was disturbed. The inlet system responded to this intervention by a net import of sediment which was eroded from the outer delta. As a consequence the tidal channels within the embayment became shallower and large bars and spits were formed. In this system, cyclic bar behaviour was observed before the closure of the Lauwers Sea (Oost 1995). In one of the major channels of the Frisian Inlet system, the Pinkegat Inlet, this cyclic behaviour was still observed after the closure; in the other major inlet, the Zoutkamperlaag Inlet, this cyclic behaviour stopped.

The mathematical–physical modelling of the interaction between water motion and the erodible bottom is a rapidly developing field of research. Originally most models were of empirical or semi-empirical type, see e.g. Van Dongeren & de Vriend (1994) and the review by de Vriend (1996). These models are (partly) based on statistical relationships between different state variables which were derived from analysing field data. At a later stage process-oriented models were developed which are based on physical principles. The first studies with such models focused on the dynamics of currents induced by tides without any feedback to morphology (Speer & Aubrey 1985; Dronkers 1986; Aubrey 1990; Parker 1991; Friedrichs & Aubrey 1994). During the last few years the morphodynamics of tidal inlets and basins have received more attention, see the review by de Vriend & Ribberink (1996). In Wang, Louters & de Vriend (1992, 1995) a numerical model was developed with which they were able to simulate present-day morphological behaviour of the Frisian Inlet and its response to the closure of the Lauwers Sea. A similar, but simpler model (based on time-integration of tidally averaged equations, see below) was developed in de Jong (1998) and applied to the Western Scheldt Estuary. Unfortunately, these models are too complex to determine the basic mechanisms responsible for the behaviour of the simulated phenomena.

This motivated Schuttelaars & de Swart (1996) to develop and analyse an idealized one-dimensional model of a short tidal embayment with a constant width. They demonstrated that for realistic parameter values this system has one morphodynamic equilibrium which is reached for arbitrary initial conditions. The bottom profile in this final state depends on the parameter values selected and is such that in the embayment a spatially uniform shear stress distribution is attained, which seems to be consistent with field observations (Friedrichs 1995). Moreover, the relation between cross-sectional area and the tidal prism appears to be linear as data indicate (de Vriend 1996). Finally, the model predicts a net import of sediment if its length is suddenly reduced, which is consistent with the behaviour of the Frisian Inlet. However, a serious limitation of this model is that it cannot explain the high morphologic activity observed in natural tidal embayments.

In this paper, it will be shown that the formation of channels and shoals may be due to an inherent positive feedback between tidal currents and the erodible bed. This will be done by investigating the stability properties of the equilibrium state of the model as discussed in Schuttelaars & De Swart (1996) within the context of a two-dimensional model. The motivation for this approach comes from studies of river dynamics in which it was found that the use of a two-dimensional model is a necessary condition for obtaining morphologic instabilities, see Schielen, Doelman & de Swart (1993) and references herein. This stability concept is also used in Seminara & Tubino (1998), but an important difference with the present study is that they consider the estuary as an open tidal river with a small ratio between the transverse

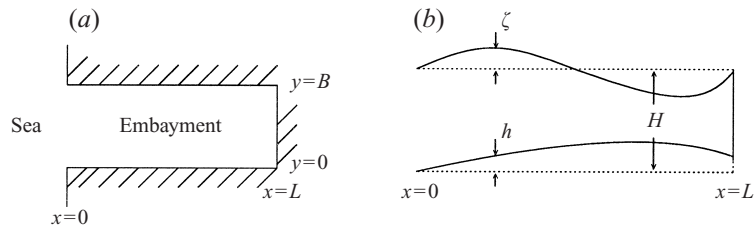


FIGURE 1. Situation sketch: (a) top view and (b) cross-sectional view of the tidal embayment.

and longitudinal length scales. On the other hand, in our model which is depth integrated, the width-to-length ratio of the embayment is considered to be finite. Hence it is designed to describe large-scale bottom patterns which are affected by the decreasing water depth of the embayment in the landward direction.

The paper is organized as follows. In §2 the model equations and boundary conditions are introduced. Depth-averaged shallow water equations are used to describe the water motion. The sediment transport model considered mainly describes the diffusive transport of suspended load. In §3, the embayment is tidally forced by the leading-order tidal constituent at the entrance of the embayment. An equilibrium state of the equations is found which is spatially uniform in the lateral direction. In §4 the stability of this equilibrium is investigated. Stability results are given and the physical mechanism is discussed. It turns out that if vorticity is not conserved two-dimensional perturbations can become linearly unstable. A preferred mode and critical conditions are found. In the last section, the results are recapitulated and discussed in the context of field observations. Moreover, some suggestions for further investigations are made.

## 2. Model description

The geometry which will be considered is that of an idealized tidal embayment of rectangular shape (width  $B$  and length  $L$ ), ignoring width variations that often strongly constrain the dynamics (Friedrichs & Aubrey 1994). The coastlines are assumed to be fixed whereas the bottom (described by  $z = -H + h$ , with  $H$  a reference depth) is erodible. The free surface is described by  $z = \zeta$  (see figure 1).

The hydrodynamic part of the equations is described by the depth-averaged shallow water equations for a homogeneous fluid (Csanady 1982; Vreugdenhil 1994), which include bottom friction terms. This set of equations is supplemented with a depth-averaged concentration equation (Van Rijn 1993), which describes sediment fluxes due to both advective and diffusive processes, and the bottom evolution equation. The bed changes due to divergences in the fluxes of suspended load and bedload sediment. As boundary conditions the free-surface elevation at the entrance of the embayment is prescribed (including tidal motions with a characteristic frequency  $\sigma$ ) and we require that there is no normal water and sediment transport at solid boundaries. Furthermore, the bottom is fixed at the entrance  $x = 0$ .

The model to be analysed in this paper aims to describe phenomena with horizontal extents which scale with the embayment length. This motivates the introduction of the following non-dimensional variables:

$$\left. \begin{aligned} x &= x^*/L, & y &= y^*/L, & u &= u^*/U, & v &= v^*/U, \\ h &= h^*/H, & t &= \sigma t^*, & \zeta &= \frac{\sigma L}{HU} \zeta^*. \end{aligned} \right\} \quad (2.1)$$

Here an asterisk refers to dimensional variables, and  $u$  and  $v$  are velocity components in the  $x$ - and  $y$ -direction, respectively. Furthermore,  $U$  is a velocity scale related to the tidal forcing at the entrance of the embayment and  $t$  is time. The width  $B$  of the embayment is assumed to be of (at most) the same order as its length. This applies to embayments like those in the Dutch Wadden Sea for which  $B/L \sim 0.2$ – $0.3$ , see table 1. This is an important difference with the model of Seminara & Tubino (1998), which describes the formation of estuarine bars in an infinitely long channel. The scale for the free-surface elevation follows from mass conservation arguments: the time derivative of the free surface should be of the same order as the divergence of the mass flux.

The result of this scaling procedure is that all nonlinear hydrodynamic terms in the shallow water equations are measured by the Strouhal number

$$\epsilon = \frac{U}{\sigma L} = \frac{\hat{\zeta}}{H}, \quad (2.2)$$

where  $\hat{\zeta}$  is a characteristic amplitude of the free-surface variations. This parameter is, apart from a factor of  $2\pi$ , the ratio of the tidal excursion and the embayment length and has usually a small value ( $\sim 0.15$  in the Wadden Sea, see table 1).

In the forthcoming analysis we assume that the tidal motion is subject to moderate bottom friction: in other words, frictional terms in the momentum equation have the same order of magnitude as local acceleration terms. Furthermore, we consider a short embayment, i.e. its length  $L$  is much smaller than  $L_g = (gH)^{1/2}/\sigma$ , which is a measure of the frictionless tidal wavelength. Finally we assume that only the leading-order tidal constituent is prescribed at the entrance. These assumptions can only be justified for a limited number of natural embayments, see the discussion at the end of this section. However, it is worth remarking that they are not necessary conditions for the general applicability of the forthcoming analysis. They are merely introduced to make this analysis as transparent as possible without excluding the essential mechanisms.

The conditions mentioned above are used to derive a simplified non-dimensional model by expanding the free surface  $\zeta$  and velocity components  $u$  and  $v$  in the small parameter  $\lambda_L^2 = L^2/L_g^2$ . At lowest order only the pressure terms in the momentum equation remain:

$$\zeta_x = 0, \quad \zeta_y = 0. \quad (2.3)$$

Here  $\zeta$  should be interpreted as the zeroth-order approximation of the free surface. The equations (2.3) describe a spatially uniform vertical tide.

Information on the zeroth-order velocity field is obtained from the  $O(\lambda_L^2)$  momentum balance: elimination of the pressure terms results in a vorticity equation. The system is closed by the continuity equation. If we neglect in these results both the nonlinear contributions and Earth rotation effects, we find

$$\zeta_t + [(1-h)u]_x + [(1-h)v]_y = 0, \quad (2.4)$$

$$v_{xt} - u_{yt} = -F_{2x}^b + F_{1y}^b, \quad (2.5)$$

with  $\mathbf{F}^b = (F_1^b, F_2^b)$  the dimensionless bottom friction vector. In principle the nonlinear contributions and Earth rotation effects can be incorporated by making additional expansions in the small parameter  $\epsilon$  and in  $f/\sigma$ , where  $f$  is the Coriolis parameter.

In order to introduce a suitable parametrization for  $\mathbf{F}^b$ , we first consider the

---

Quantities in the dimensional model		
$H \sim 10 \text{ m}$	$L \sim 2 \times 10^4 \text{ m}$	$B \sim 2\text{--}5 \times 10^3 \text{ m}$
$\hat{\zeta} = \frac{HU}{\sigma L} \sim 1.5 \text{ m}$	$\sigma \sim 1.4 \times 10^{-4} \text{ s}^{-1}$	$L_g \sim 1.5 \times 10^5 \text{ m}$
$\alpha \sim 10^{-2} \text{ kg s m}^{-4}$	$\gamma \sim 4 \times 10^{-3} \text{ s}^{-1}$	$\mu_* \sim 10^2 \text{ m}^2 \text{ s}^{-1}$
$r_* \sim 10^{-3} \text{ m s}^{-1}$	$\rho_s \sim 2650 \text{ kg m}^{-3}$	$p \sim 0.4$
$u_c \sim 0.3 \text{ m s}^{-1}$	$\hat{s} \sim 3 \times 10^{-6} \text{ m}^2 \text{ s}^{-1}$	$\kappa_* \sim 2$
Parameters in the non-dimensional model		
$\epsilon \sim 0.15$	$a \sim 0.04$	$\mu \sim 1.8 \times 10^{-3}$
$\delta_s \sim 8 \times 10^{-4}$	$\delta_b \sim 5.4 \times 10^{-7}$	$\lambda \sim 6.8 \times 10^{-7}$
$\lambda_L^2 \sim 0.02$	$r \sim 0.7$	

TABLE 1. Quantities and parameter values for the Frisian inlet system. The symbols are explained in the text.

---

dimensional friction vector

$$\mathbf{F}_*^b = -\frac{\tau_*^b/\rho}{H-h+\zeta}$$

with  $\tau_*^b$  the bed shear stress and  $\rho$  the density of the water. Both observations and dimension analysis indicate that the bed shear stress is a quadratic function of the velocity. However, our main objective is not to give a detailed description of the tidal flow but rather to study its gross features. Therefore we adopt a linear friction law which reads in dimensional units

$$\tau_*^b = \rho r_* \mathbf{u}, \quad (2.6)$$

where  $r_*$  is a friction parameter with units  $\text{m s}^{-1}$ . This choice avoids the complications which result from the application of a quadratic friction law, without neglecting the essential physics of the problem. The parameter  $r_*$  is chosen such that the net dissipation of energy (averaged over the tidal cycle and embayment) due to the linearized shear stress (2.6) equals that of the bed shear stress based on the quadratic friction law. More details on this procedure are given in Lorentz (1922) and Zimmerman (1982, 1992). It implies that  $r_*$  is proportional to the tidal current amplitude  $U$  and the bottom roughness. This will be used later on in this paper. Typical values for  $r_*$  in tidal embayments are  $O(10^{-3} \text{ m s}^{-1})$ . This implies that in the present non-dimensional model  $\mathbf{F}_*^b = r\mathbf{u}/(1-h)$  where  $r = r_*/(H\sigma)$ . Characteristic values for  $r$  are  $O(0.1\text{--}1)$ .

A serious limitation of this parametrization is that the friction terms become unbounded if the water depth tends to zero, as observed near tidal flats. As our model is designed to give only a global description of the tidal flow in an embayment, the friction term is replaced by its Taylor series:

$$\mathbf{F}_b = r\mathbf{u}(1 + \eta h + \eta^2 h^2 + \dots). \quad (2.7)$$

If  $\mathbf{F}_b$  is truncated after the first term there are no sources of vorticity, hence the non-transient flow will be irrotational. If the dependence on the bed level is included a mechanism to produce vorticity is introduced. Formally  $\eta$  should have a value of 1. As will be shown, the essential physics is already accounted for by including only two

terms in the Taylor expansion. In what follows we use  $\mathbf{F}_b = \mathbf{ru}(1 + \eta h)$ , where  $\eta = 0$  corresponds to the irrotational case and  $\eta = 1$  to the situation in which vorticity can be produced.

Next we turn to the concentration equation which describes the transport of suspended sediment. Here a depth-integrated equation is used which is an inhomogeneous advection–diffusion equation, see Van Rijn (1993) for details. The source and sink terms are due to the pick-up and deposition of sediment near the bottom, respectively. Both from field observations (Dyer & Soulsby 1988) and from theoretical considerations it is known that the sediment pick-up term will be some power of the absolute velocity. Here we choose (in dimensional units) a quadratic parametrization:

$$\text{Sediment pick-up term} = \alpha ((u^*)^2 + (v^*)^2)$$

where  $\alpha$  is a constant which depends on the sediment characteristics. For fine sand (grain size  $2 \times 10^{-4}$  m) a typical value is  $\alpha \sim 10^{-2} \text{ kg m}^{-2} \text{ s}^{-1}$ . At this point it is useful to remark that choosing any other exponent ( $\geq 1$ ) of the absolute velocity would yield qualitatively similar results. The deposition of sediment is proportional to the depth-integrated concentration  $C^*$  (amount of sediment in a water column with unit area) and measured by a coefficient  $\gamma$ . The quantity  $\gamma^{-1}$  defines the e-folding time scale of the deposition process which for fine sand is of the order of 250 s. Now a scale for the concentration follows from the fact that in near-equilibrium conditions there is an approximate balance between the pick-up and deposition of sediment. Thus a non-dimensional depth-integrated concentration can be defined as  $C = \gamma C^*/(\alpha U^2)$  where the asterisk denotes the dimensional variable. If also the definitions (2.1) and the assumptions discussed earlier are used we obtain the concentration equation

$$aC_t = (u^2 + v^2) - C + a\mu[C_{xx} + C_{yy}], \quad (2.8)$$

Here  $a = \sigma/\gamma$  is the ratio of the deposition time scale and the tidal period (for medium sand  $a \sim 10^{-2}$ ). The dimensionless horizontal diffusion coefficient  $\mu$  is defined by  $\mu = \mu_*/\sigma L^2$ , the ratio of the tidal period and the diffusive time scale with typical values of  $O(10^{-2} - 10^{-3})$ . Note that here also advective terms have been neglected. As demonstrated in Schuttelaars & de Swart (1996) this is only a valid assumption in the case of a short embayment.

The final equation to be considered is the bottom evolution equation which can be derived from mass conservation. According to the discussions in Dyer (1986), Fredsoe & Deigaard (1992) and Van Rijn (1993) changes in the bed level are due to a local difference between the sediment pick-up and deposition fluxes near the bottom. This process, which is related to suspended load transport, takes place on a morphologic time scale  $T_s$ , which appears to be given by  $\rho_s(1-p)H/(\alpha U^2)$ . Here  $\rho_s$  is the density of the individual grain particles and  $p$  the bed porosity. From table 1 it appears that for natural embayments  $T_s$  is much larger than the tidal period.

Furthermore the bottom evolution is forced by local divergences in the volumetric sediment flux per unit width, which is related to bedload transport. The corresponding time scale is  $T_b = (\sigma HL)/\hat{s}(u_c/U)^b$  with  $u_c$  the critical velocity for sediment pick-up and  $\hat{s}$  a function of the sediment properties. This bedload flux consists of an advective part, which is independent of the bed level, and a part which is proportional to the local bottom slope. This latter part describes the tendency of the sediment to move downslope and its effect is measured by a parameter  $\kappa_* \sim 2$ .

In the systems under study the time scale  $T_b$  is much larger than  $T_s$ , hence the bedload flux is much smaller than the suspended load fluxes. However bedload effects

cannot be neglected because they appear to have a substantial effect on the behaviour of small-scale bedforms.

The fact that both the morphodynamic time scales  $T_s$  and  $T_b$  are much longer than the hydrodynamic time scale  $\sigma^{-1}$  implies that the bed level  $h$  is a slow variable. Consequently the method of averaging can be used: the bottom variable  $h$  may be considered stationary on the short tidal time scale and its evolution is determined only by the net sediment transports averaged over a tidal cycle. The mathematical foundations of this approach are discussed in Sanders & Verhulst (1985) and Krol (1991). It then appears that in the present model the tidal average of the advective part of the volumetric sediment flux is zero; only the slope term yields a contribution. This seems to be consistent with flume experiments of Talmon, Mierlo & Struiksmas (1995) which show that slope effects are very important for suspended load dominated transport.

This results in the following dimensionless bottom evolution equation:

$$h_\tau = -\langle (u^2 + v^2) - C \rangle + \lambda \langle \nabla^2 (h - h_{\text{eq}}) \rangle \quad (2.9)$$

Here  $\tau = \delta_s t$  is a slow time coordinate and  $\delta_s = (\sigma T_s)^{-1} \ll 1$  is the ratio of the hydrodynamic time scale and morphologic time scale  $T_s$ . The terms on the right-hand side describe the contributions due to the suspended load and bedload, respectively. Here  $\lambda = \kappa_* H \delta_b / (L \delta_s)$  which is a small parameter (see table 1),  $\delta_b = (\sigma T_b)^{-1}$  and  $h_{\text{eq}}$  an as yet unspecified equilibrium profile of the equations.

Note that the bedload term in (2.9) only gives a contribution if the bottom is perturbed from an equilibrium  $h_{\text{eq}}$ . This means that in morphodynamic equilibrium there is no bedload transport due to bottom slopes. Thus, it is implicitly assumed that in equilibrium the fluxes due to slope effects (usually seaward directed) are compensated by wave-induced landward fluxes. However, if the system is perturbed, bottom fluxes give a (small) contribution. A similar approach is used in a study by Falqués, Montoto & Iranzo (1996) on the dynamics of bedforms in the surf zone.

The boundary conditions at the fixed coastlines are given by

$$(1 - h)\mathbf{u} \cdot \mathbf{n} = 0, \quad \mu \nabla C \cdot \mathbf{n} = 0, \quad \lambda \nabla h' \cdot \mathbf{n} = 0 \quad \text{at } x = 1, y = 0, y = \frac{B}{L}, \quad (2.10)$$

where  $\mathbf{n}$  is the normal vector and  $h' = h - h_{\text{eq}}$ . They require the normal fluxes of water and sediment to vanish at these locations. At the open boundary, the conditions read

$$\zeta = \cos(t), \quad S = 0, \quad h = 0 \quad \text{at } x = 0 \quad (2.11)$$

with  $S = (u^2 + v^2) - C$ . Note that there are no spatial shifts in the free-surface elevation across the entrance. This is a consequence of the fact that the width of the embayment is much smaller than the tidal wavelength. The two other conditions imply a balance between erosion and deposition and a fixed bottom at this location. The latter is a severe condition because it implies that the bottom at the entrance is not affected by the sediment exchange between the embayment and the adjacent sea. In order to investigate this aspect a more complicated model geometry would be required, which is beyond the scope of this paper.

Using the original dimensionless shallow water equations for a short embayment, it follows that the  $O(\lambda_1^2)$  momentum balance in the transverse direction reduces to  $v_t = -F_2^b$ . Here nonlinear and Coriolis terms are again neglected. Since  $F_2^b \sim v$  it follows that non-transient solutions also obey  $v = 0$  at  $x = 0$ .

As an example of an embayment under study, consider the main channel of the Frisian inlet system (Wang *et al.* 1992, 1995). It has an approximate length of 20 km and a depth of 10 m and the forcing is largely due to the  $M_2$  tide. The sediment

in the channel is fine sand with a grain size of  $2 \times 10^{-4}$  m. A typical value for the horizontal diffusion coefficient is  $\mu_* \sim 100 \text{ m}^2 \text{ s}^{-1}$ , as discussed in e.g. Ridderinkhof & Zimmerman (1992). Some other useful quantities are listed in the first part of table 1; in the second part of this table, the dimensionless parameters are listed.

### 3. Basic state

As described by (2.11), the system is forced at the entrance of the embayment. Using (2.3) it is easily seen that

$$\zeta(x, y, t) = \cos t, \quad (3.1)$$

which describes a spatially uniform tide in the embayment.

We now investigate the existence of an equilibrium state which has no structure in the  $y$ -direction (hence all quantities are independent of  $y$ ) and which has no velocity component in the  $y$ -direction. The equations (2.4), (2.8) and (2.9) reduce to

$$-\sin t + [(1 - h_{\text{eq}})u_{\text{eq}}]_x = 0, \quad (3.2a)$$

$$a(C_{\text{eq}t} - \mu C_{\text{eq}xx}) = u_{\text{eq}}^2 - C_{\text{eq}}, \quad (3.2b)$$

$$\langle u_{\text{eq}}^2 - C_{\text{eq}} \rangle = 0, \quad (3.2c)$$

where we have used that in equilibrium no bedload transport is present (see §2). Furthermore, we used that  $\mathbf{F} \sim \mathbf{u}$  (linear friction law), so the vorticity equation (2.5) is automatically obeyed since  $v = 0$  and  $u$  is only a function of  $x$ . A solution of (3.2a) is

$$u_{\text{eq}} = -\sin t, \quad v_{\text{eq}} = 0, \quad (3.3a)$$

$$C_{\text{eq}} = \frac{1}{2} - \frac{a}{1 + 4a^2} \left[ \frac{1}{2a} \cos 2t + \sin 2t \right], \quad h_{\text{eq}} = x. \quad (3.3b)$$

This equilibrium profile represents a constantly sloping bottom with a spatially uniform velocity field. This means that the one-dimensional profile  $h_{\text{eq}} = x$  is an equilibrium profile of the two-dimensional equations as well. It is not clear whether or not this equilibrium is stable. In Schuttelaars & de Swart (1996) it has been shown that without gravitational effects,  $h_{\text{eq}}$  is linearly stable with respect to small, one-dimensional perturbations. They also showed, using numerical experiments that this equilibrium profile is globally stable with respect to one-dimensional perturbations. Here we will focus on the stability properties of the basic state with respect to two-dimensional perturbations.

### 4. Two-dimensional perturbations

Consider perturbations which evolve on the equilibrium as given in §3. Using (2.3) and the boundary condition for the free-surface elevation (2.11) it is easily seen that the perturbations  $\zeta'$  are always zero. Thus in the equations of motion the following expressions are substituted:

$$\Phi = \Phi_{\text{eq}} + \Phi' \quad (4.1)$$

where  $\Phi = (\zeta, u, v, C, h)^T$  is the solution vector,  $\zeta' = 0$  and  $\Phi_{\text{eq}}$  is given in (3.3). In (4.1), the superscript  $'$  labels the perturbations, which are considered to be small

with respect to the basic variables. Next, the continuity equation (2.4) and the vorticity equation (2.5) are linearized with respect to these perturbations. This results in

$$[(1-x)u' + h' \sin t]_x + (1-x)v'_y = 0, \quad (4.2a)$$

$$v'_{ix} - u'_{iy} = -\tilde{F}_{2x}^b + \tilde{F}_{1y}^b, \quad (4.2b)$$

where  $\tilde{F}^b$  is the linearized bottom friction vector (2.7) which includes only the first two terms in the Taylor expansion. The corresponding boundary conditions are derived from (2.10)–(2.11) and read

$$(1-x)u' + h' \sin t = 0 \quad \text{at } x = 1, \quad (4.3a)$$

$$v' = 0 \quad \text{at } y = 0, y = \frac{B}{L}, x = 0. \quad (4.3b)$$

The latter condition was discussed in §2. Thus (4.2)–(4.3) govern the dynamics of the flow perturbations for a given bottom disturbance. Next the sediment transport and sediment balance are considered. In the concentration equation, only the tidally averaged concentration  $\mathcal{C}'$  is dynamically significant. The equation that describes the non-fluctuating part of the concentration reads after linearization

$$-\delta^2 \mathcal{C}'_{xx} - \delta^2 \mathcal{C}'_{yy} = -\langle 2u' \sin t \rangle - \mathcal{C}' \quad (4.4)$$

where  $\delta = (a\mu)^{1/2} = (\mu_*/\gamma)^{1/2}/L$  is the ratio of the diffusive length scale and the embayment length. Linearizing the bottom evolution equation yields

$$h'_\tau = \langle 2u' \sin t \rangle + \mathcal{C}' + \lambda \nabla^2 h'. \quad (4.5)$$

The boundary conditions are

$$\langle 2u' \sin t \rangle + \mathcal{C}' = 0, \quad h' = 0 \quad \text{at } x = 0, \quad (4.6a)$$

$$\frac{h'}{1-x} \text{ finite}, \quad \mathcal{C}'_x + \lambda h'_x = 0 \quad \text{at } x = 1, \quad (4.6b)$$

$$\delta^2 \mathcal{C}'_y = 0, \quad \lambda h'_y = 0 \quad \text{at } y = 0, y = \frac{B}{L}. \quad (4.6c)$$

The boundary conditions at the landward side of the embayment ( $x = 1$ ) require some explanation. They are due to the fact that the undisturbed water depth described by the basic state becomes zero at this position. Since we require bounded solutions at this weakly singular point, the first condition follows directly from (4.3a) by requiring that  $u'$  must be finite at  $x = 1$ . Furthermore, at this point no distinction can be made between suspended and bedload transport. Consequently, the total load transport has to vanish.

Now the structure of equations (4.2a), (4.2b), (4.4) and (4.5) and the boundary conditions on the fixed walls imply that the solutions can be written as

$$u' = \sum_{n=0}^{\infty} [u_n^c(x) \cos t + u_n^s(x) \sin t] \cos(l_n y), \quad (4.7a)$$

$$v' = \sum_{n=0}^{\infty} [v_n^c(x) \cos t + v_n^s(x) \sin t] \sin(l_n y), \quad (4.7b)$$

$$\mathcal{C}' = \sum_{n=0}^{\infty} C_n(x) \cos(l_n y), \quad (4.7c)$$

$$h' = \sum_{n=0}^{\infty} h_n(x) \cos(l_n y), \quad (4.7d)$$

with  $l_n = n\pi L/B$  and  $n = 0, 1, 2, \dots$ . Thus, the lateral spatial structure of the state variables can be expanded in Fourier modes with wavenumber  $l_n$ .

Whenever  $\eta \neq 0$  in the friction vector (2.7), the frictional terms couple the  $\sin t$  and  $\cos t$  components of the perturbed velocity field  $\mathbf{u}'$  in (4.7). In that case phase shifts in time act between velocity components, which can result in a net sediment transport from troughs to crests of bedforms and hence positive growth rates of the perturbations are found.

Using (4.2a), (4.2b) and (4.7), the linearized continuity equations read

$$[(1-x)u_n^s]_x + h_{nx} + l_n(1-x)v_n^s = 0, \quad (4.8a)$$

$$[(1-x)u_n^c]_x + l_n(1-x)v_n^c = 0, \quad (4.8b)$$

and the vorticity equations are given by

$$v_{nx}^s + l_n u_n^s + r l_n [1 + \eta x] u_n^c + r [1 + \eta x] v_{nx}^c + \eta r v_n^c = 0, \quad (4.9a)$$

$$v_{nx}^c + l_n u_n^c + \eta r l_n h_n - r l_n [1 + \eta x] u_n^s - r [1 + \eta x] v_{nx}^s - \eta r v_n^s = 0, \quad (4.9b)$$

with boundary conditions which can be derived from (4.3a).

Using the expansions (4.7), the concentration equation becomes

$$\delta^2 C_{nxx} - (1 + \delta^2 l_n^2) C_n = u_n^s \quad (4.10)$$

and the bottom evolution equation reads

$$h_{n\tau} = (u_n^s + C_n) + \lambda (h_{nxx} - l_n^2 h_n) \quad (4.11)$$

with the boundary conditions to be derived from (4.6).

Solutions of this system of equations are of the form

$$\Psi' = \text{Re} \{ (u_n^s, u_n^c, v_n^s, v_n^c, C_n, h_n) e^{\omega \tau} \}$$

with  $\omega$  a complex frequency. Here  $\text{Re}$  denotes the real part,  $\text{Re}[\omega]$  is the exponential growth rate and  $\text{Im}[\omega]$  the frequency. Substitution in (4.8)–(4.11) with corresponding boundary conditions defines an eigenvalue problem, which is solved by a finite difference technique (central method). The introduction of  $\Psi = (\Psi'_1, \Psi'_2, \dots, \Psi'_N)$  where  $\Psi'_i$  is  $\Psi'$  evaluated at gridpoint  $i$  yields the set of algebraic equations

$$\mathbf{A}\Psi = \omega \mathbf{B}\Psi.$$

Here  $\mathbf{A}$  is a  $6N \times 6N$  matrix with elements which depend on the parameters  $\delta, r, \eta, l_n$  and  $\lambda$ . The  $6N \times 6N$  matrix  $\mathbf{B}$  has only  $N$  non-zero elements which are on the diagonal and have the value 1. Their row numbers correspond to the equation describing the bottom evolution.

The solutions of this eigenvalue problem are obtained by using standard numerical packages. The eigenfunctions  $\Psi'$  and eigenvalues  $\omega$  depend on the parameters  $\delta, r, \lambda, l_n$  and  $\eta$ . The non-dimensional diffusion parameter  $\delta$  is determined by the sediment properties and the embayment length and the friction parameter  $r$  by the tidal velocity amplitude, tidal frequency and water depth. The bedslope coefficient  $\lambda$  is controlled by the sediment properties and by the length-to-width ratio of the embayment. Finally  $l_n$  depends on the length and width of the embayment. The parameter  $\eta$  is not a real physical parameter and will be chosen to be either 0 or 1. The stability of the system

with different parameter settings will be studied in the next sections. However, one has to be careful in varying the parameters: if for example the diffusion coefficient  $\delta$  is changed by selecting different sediment properties, the parameter  $\lambda$  and the slow time coordinate  $\tau$  must be changed as well. Therefore, it is difficult to compare results when only  $\delta$  is changed while the time scale and the bedslope coefficient are kept fixed. However, the width  $B$  only enters in the definition of the parameter  $l_n$  and a different tidal velocity results in a different friction parameter  $r$ . So in subsequent sections, the stability of perturbations is studied for different embayment widths by varying  $l_n$  (keeping  $L$  fixed) and for different tidal velocities by varying  $r$ . Some additional remarks will be made on the influence of the diffusion coefficient  $\delta$  and the bedslope parameter  $\lambda$  on the stability properties.

## 5. Potential flow and related bottom profiles

In this section we will consider an irrotational velocity field, i.e.  $\eta = 0$  in (4.9). It serves as an illustrative and transparent example of the power of this method and has the advantage that analytical solutions for the flow and concentration field can be found which is not possible in the case  $\eta \neq 0$ .

From (4.8) and (4.9), it is easily seen that  $\{u_n^s, v_n^s\}$  and  $\{u_n^c, v_n^c\}$  decouple. The equations for  $\{u_n^s, v_n^s\}$  read

$$[(1-x)u_n^s + h_n]_x + l_n(1-x)v_n^s = 0, \quad (5.1a)$$

$$v_{nx}^s + l_n u_n^s = 0. \quad (5.1b)$$

The equations for  $\{u_n^c, v_n^c\}$  are of no interest from a morphodynamical point of view, because they do not result in net erosion or deposition of sediment in the linearized bottom evolution equation. Therefore, we will focus on (5.1), supplemented with (4.10) and (4.11).

In this case an eigenvalue problem in  $h$  can be derived by expressing  $u_n^s, v_n^s, C$  in terms of  $h$ . First, the hydrodynamical part of the equations will be solved. A differential equation for  $v_n^s$  is obtained by substituting (5.1b) in (5.1a). The resulting equation reads

$$v_{nxx}^s - \frac{v_{nx}^s}{1-x} - l_n^2 v_n^s = l_n \frac{h_{nx}}{1-x}, \quad (5.2)$$

which is an inhomogeneous Bessel differential equation (Abramowitz & Stegun 1965). Note that the width-to-depth ratio is still present in the equations, namely in the parameter  $l_n$ .

The solution can be found by e.g. the variation-of-constant method and reads

$$v_n^s = \left[ A_n I_0(l_n \xi) + B_n K_0(l_n \xi) + l_n K_0(l_n \xi) \int_0^\xi I_0(l_n w) h_{nw} dw - l_n I_0(l_n \xi) \int_0^\xi K_0(l_n w) h_{nw} dw \right]. \quad (5.3)$$

Using (5.1b), the profile in the  $x$ -direction of the longitudinal velocity reads

$$u_n^s = l_n \left[ A_n I_1(l_n \xi) - B_n K_1(l_n \xi) - l_n K_1[l_n \xi] \int_0^\xi I_0(l_n w) h_{nw} dw - l_n I_1(l_n \xi) \int_0^\xi K_0(l_n w) h_{nw} dw \right] \quad (5.4)$$

with  $I_{0,1}$  and  $K_{0,1}$  the first- and second-order modified Bessel functions of index 0, 1, respectively (see Abramowitz & Stegun 1965) and  $\xi = 1 - x$ .

The constants  $A_n$  and  $B_n$  are determined by the boundary conditions. Application of (4.3a) and (4.6) yields

$$B_n = h_n|_{\xi=0} = 0$$

and from (4.3b) it follows that

$$A_n = -l_n \frac{K_0(l_n)}{I_0(l_n)} \int_0^1 I_0(l_n w) h_{nw} dw + l_n \int_0^1 K_0(l_n w) h_{nw} dw. \quad (5.5)$$

Now consider the concentration equation (4.10) with its boundary conditions. This equation can also be solved with the variation-of-constant method and reads

$$C_n = A e^{-\xi/\beta} + B e^{-(1-\xi)/\beta} - \frac{\beta}{2\delta^2} \int_0^1 e^{-(|\xi-z|)/\beta} u_n^s dz \quad (5.6)$$

with  $\beta = \delta/(1 + \delta^2 l_n^2)^{1/2}$  and

$$B = \frac{e^{-1/\beta} \left[ \lambda h_\xi(\xi = 0) - \frac{\beta}{\delta^2} \int_0^1 \sinh\left(\frac{z}{\beta}\right) u_n^s dz \right] - u_n^s(\xi = 1)}{1 + e^{-2/\beta}}, \quad (5.7)$$

$$A = B e^{-1/\beta} + \lambda h_\xi(\xi = 0) - \frac{\beta}{2\delta^2} \int_0^1 e^{-z/\beta} u_n^s dz. \quad (5.8)$$

Using the expressions for  $u_n^s$  and  $C_n$ , we can solve the bottom evolution equation:

$$h_{n\tau} = (u_n^s + C_n) + \lambda (h_{n\xi\xi} - l_n^2 h_n). \quad (5.9)$$

Note that this results in an integro-differential equation which cannot be solved analytically anymore. Therefore, a numerical method is used similar to the one described in the previous section. The procedure in this case is to write  $\mathbf{h} = (h_1^*, \dots, h_N^*) e^{\omega\tau}$  where  $h_i^*$  is the value of  $h_n$  at grid point  $i$ . Furthermore, the integral expression (5.6) is discretized and the resulting grid values are written as  $C_i^* = \sum_j C(i, j) h_j^*$  with  $C(i, j)$  an  $N \times N$  matrix. Now the following eigenvalue problem is obtained:

$$\omega \mathbf{h} = L(x(i), C(i, j), \delta, \lambda) \mathbf{h}$$

which is solved with standard numerical tools. Note that, because the hydrodynamic equations are solved in closed form, the only unknown variable in the eigenvalue problem is the bottom function  $\mathbf{h}$ , whereas in the rotational case all hydrodynamic quantities appear in the eigenvalue problem, resulting in a different kind of problem (see §4).

### 5.1. No gravitational bedload effects

In figure 2 the first three eigenvalues, which correspond to different longitudinal modes, are plotted as functions of the lateral wavenumber  $l_n$  by varying the width of the embayment (see the discussion in §4). In the numerical experiments, we have selected  $\delta = 0.01$  and  $\lambda = 0$ , for a motivation of these values see table 1. It appears that the eigenvalues are real and negative for all values of the parameter  $l_n$  so that there is no morphodynamic instability mechanism in this case. Note that the parameter  $l_n = n\pi L/B$ . This is, in fact, not a continuous parameter as  $n$  can only take integer values.

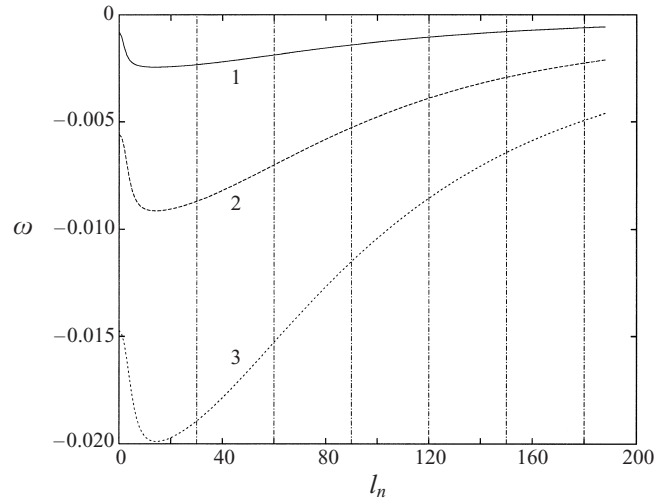


FIGURE 2. Plot of the first three eigenvalues for different values of  $l_n$  with  $\lambda = 0$  and  $\delta = 0.01$  (irrotational flow model). The vertical lines indicate the values which  $l_n$  can attain for  $L/B = 30/\pi$ .

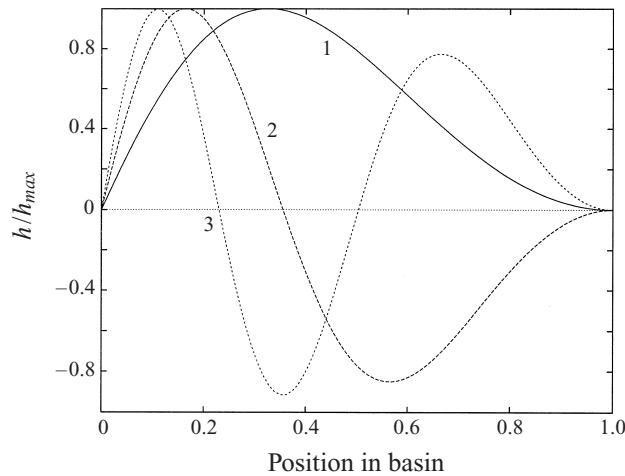


FIGURE 3. First three eigenmodes of the bottom for  $l_2 = 60$  with  $\lambda = 0$  and  $\delta = 0.01$ .

Hence by fixing the length  $L$  and the width  $B$  of the embayment, a discrete number of eigenmodes in the  $y$ -direction is obtained. In figure 2 this is indicated by the dashed vertical lines which correspond to the realistic choice  $\pi L/B = 30$ , see table 1. The one-dimensional case corresponds to  $n = 0$ . In figure 3 the longitudinal structure of the first three eigenmodes with  $l_2 = 60$  is plotted.

In figure 4(a) this structure is shown for different values of  $l_n$  for the first eigenmode. Results for the concentration profile are presented in figure 4(b). In these figures, all quantities are scaled to 1; in table 2 the maxima of the different physical quantities are given.

We now describe what happens if the parameter  $l_n$  is increased: first, it appears that the concentration profile and the velocity profile in the  $x$ -direction are almost identical; they only have a different sign. This is to be expected for  $\delta l_n \ll 1$  because no large derivatives in  $C_n$  are encountered (see figure 4b) and hence the difference between

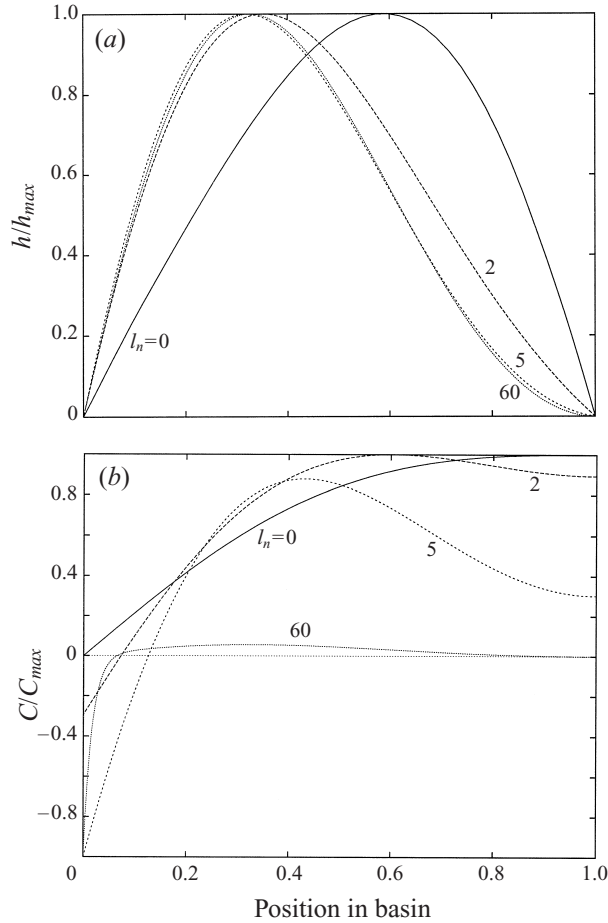


FIGURE 4. Plot of the eigenfunctions for  $\delta = 0.01$  and  $\lambda = 0$ . The irrotational case. (a) First eigenmode for the bottom  $h_n$  for different  $l_n$ -values. (b) First eigenmode for the concentration  $C_n$  for different  $l_n$ -values.

---

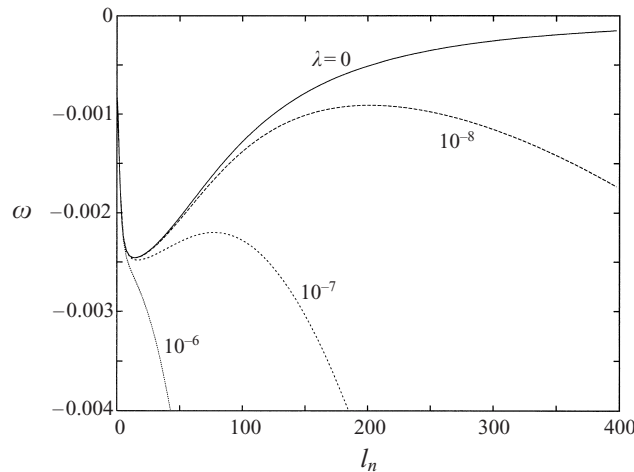
Wavenumber $l_n$	$h_{max}$	$C_{max}$	$u_{max}^s$	$v_{max}^s$
0	1	2.27	2.27	0
2	1	1.26	1.27	1.84
5	1	0.57	0.57	1.29
60	1	0.09	0.09	0.12

---

TABLE 2. Maxima of the various physical quantities for different values of  $l_n$  (first longitudinal mode); irrotational flow model.

---

the perturbed sediment pick-up flux and the perturbed deposition flux (described by  $C_n$ ) is of order  $\delta^2$  (see (4.10)). For  $\delta^2 l_n^2 \sim 1$  this is no longer true, because the lateral diffusion of sediment in (4.10) is now of the same order as the perturbed sediment pick-up and deposition terms. In order to obey the boundary condition at the entrance a diffusive boundary layer in this region is formed (see figure 4(b)). From the concentration equation we see that the width of the boundary layer near  $x = 0$  is

FIGURE 5. The first eigenvalue for different values of  $\lambda$ .

of  $O(1/l_n)$ . For even larger wavenumbers ( $\delta l_n \gg 1$ ) only the diffusion terms in (4.10) are dynamically significant and the width of the boundary layer near  $x = 0$  is of  $O((\delta l_n)^{-1})$ .

Note that with increasing values of the lateral wavenumber  $l_n$  of the perturbation the maximum of  $C_n$  shifts from the landward to the seaward boundary and the bottom perturbation becomes smaller near the landward boundary.

At this point we want to emphasize that the asymptotic expansion for  $C_n$  in the small parameter  $\delta$ , as used in Schuttelaars & de Swart (1996) for the case  $l_n = 0$ , is not correct for  $l_n$  too large. This is because in the expansion of the concentration  $C_n$  it is assumed that all derivatives of the resulting eigenfunctions are of order one. This assumption is correct for  $\delta l_n \ll 1$  but is violated for larger  $l_n$ . The results obtained by using this (incorrect) asymptotic expansion of the complete solution differ considerably: the eigenvalues turn out to be complex and have a positive real part, hence the basic state is unstable. The corresponding eigenfunctions are very spiked near the entrance of the embayment, thus violating the assumption underlying the asymptotic expansion. Therefore one must be very careful when analysing the concentration equation in the case of two-dimensional perturbations. For more details, see Schuttelaars (1997).

Finally, we point out that there is a problem with the results obtained by solving the complete concentration equation as well: from figure 2 it is clear that the fast oscillating modes (i.e. with large mode number  $n$ ) become marginally stable (see also the Appendix, §A.1). This is inconsistent with the use of the shallow water equations which are based on the assumption that small-scale features are dynamically insignificant. This motivates the introduction of slope effects in the sediment transport formulation which is the subject of the next section.

### 5.2. Bedload transport incorporated

We now assume that the bedslope parameter  $\lambda$  has non-zero values. It is seen (figure 5) that for large values of  $l_n$  the eigenvalues of the bottom perturbation become more negative and hence the basic state becomes more stable with respect to these perturbations. This is to be expected because slope effects cause the damping of small-scale perturbations, see also the Appendix, §A.1.

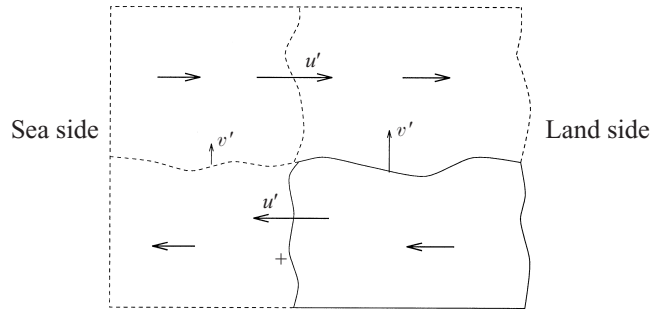


FIGURE 6. Sketch which corresponds to a necessary situation for instability during flood. The arrows indicate the direction and magnitude of the perturbed velocities  $u'$  and  $v'$ . The bottom perturbation is positive at the plus sign and negative at the minus sign. For a more complete discussion, see the text.

### 5.3. Physical interpretation

In the case of potential flows no perturbations of the basic state with positive growth rate were found. To understand the stabilizing mechanism, the bottom evolution equation is rewritten with the use of the concentration equation, as

$$h'_\tau = -\nabla \cdot \mathbf{F} \quad (5.10)$$

where  $\mathbf{F} = (F_1, F_2)$  is the perturbed total load sediment flux with components

$$F_1 = -\delta^2 \langle C' \rangle_x - \lambda h'_x, \quad F_2 = -\delta^2 \langle C' \rangle_y - \lambda h'_y. \quad (5.11)$$

The general condition for instability is that there is a net transport from the trough regions (where  $h' < 0$ ) to the crest regions ( $h' > 0$ ). In the present diffusive model this requires larger concentrations in the trough regions than in the crest regions. The resulting net convergence (divergence) of the diffusive suspended load flux in the crest (trough) region should be large enough to overcome the stabilizing effects of the slope terms in the total load flux.

Since, to a good approximation,  $\mathcal{C}' \sim \langle 2u_{\text{eq}}u' \rangle$  (or  $C_n \sim -u_n$ , see the discussion in § 5.1), this implies that the sediment pick-up must be large in the troughs and small over the crests. Consequently, the longitudinal velocity component  $u = u_{\text{eq}} + u'$  must decrease if the tidal flow moves upslope and increase if the flow moves downslope.

When the flow is irrotational, as studied in this section, instability behaviour is not to be expected because the only tide-topography interaction mechanism is due to continuity effects (i.e. mass conservation) which requires the tidal flow to increase when moving upslope. This can be easily seen in the case of the one-dimensional model: the continuity equation (4.2a) then shows that  $u'/u_{\text{eq}} = h'/(1-x)$ , hence there are high erosion rates at the crests and low erosion rates in the troughs. Thus there can be no instability.

This statement also holds when the perturbations are two-dimensional and the flow is irrotational. Consider for this purpose the situation in figure 6 which shows the distribution of the perturbed longitudinal velocity component, required for unstable behaviour near the entrance of the embayment during flood. The ebb situation follows by reversing all signs. For convenience a bar is selected near  $y = 0$ . It appears that in the region under study  $\partial u'/\partial y$  must be positive. For irrotational flows, this implies positive  $\partial v'/\partial x$  and (since  $v' = 0$  at the entrance) also  $v' > 0$ . Now consider only the downslope area (which is the region inside the solid line in figure 6) which is bounded by  $y = 0$ , a line  $y > 0$  where  $u' = 0$  (or, if such a curve does not exist, the line  $y = B/L$  is chosen), a curve that indicates where  $h_x = 0$ , and the right-hand boundary is given

by the condition that  $u' = 0$  (which can always be found). At the lower boundary the water flux is zero since  $v' = 0$  here and at the upper boundary there is an outward water flux. At the left-hand boundary  $u' < 0$ , implying that  $(1 - x)u' < 0$ , and  $h' > 0$  which means that  $-u_{\text{eq}}h' < 0$ . Hence at this boundary there is an outward flux since  $\partial v'/\partial x > 0$  and  $v' > 0$ . At the right-hand boundary  $u' = 0$  and  $h' = 0$  which means that there is no water flux through this boundary. Collecting all flux contributions, it is clear that there is a net water flux out of the area under study. Thus in this area, mass conservation is violated, which means that the assumption about distribution of the perturbed velocity component  $u'$  is incorrect. Since this velocity distribution was essential to have morphodynamic instabilities, no instabilities can develop.

In order to understand and interpret the results obtained so far, let us study the feedback between the tidal flow and the bottom in more detail. In figure 7(a) the longitudinal sediment flux  $F_1$  for the  $n = 0$  mode is plotted which is related to the bottom profile denoted by  $h$ . It appears that at the crests  $F_{1x} > 0$ , which means net erosion, whereas above the troughs  $F_{1x} < 0$ , which means net deposition. Hence, there is a net diffusive transport from crest to trough, resulting in a negative feedback mechanism. Since there is no variation in the  $y$ -direction, no lateral sediment flux is found.

In figure 7(b) the sediment flux  $F_1$  for the mode with  $l_n = 60$  is plotted; the corresponding bottom profile  $h$  is also shown. Note that at the sea side of the embayment the flux becomes very large but remains finite. It is observed that the sediment flux in the  $x$ -direction is not stabilizing throughout the entire embayment (as was the case when  $n = 0$ ): at the entrance of the embayment, a net erosion due to a flux in the  $x$ -direction is found; at the end of the embayment a net deposition occurs. Therefore, the perturbation at the entrance becomes smaller and at the end of the embayment larger. However, figure 7(b) only shows the sediment flux in the  $x$ -direction. Since  $l_n \neq 0$ , there is a flux in the lateral direction as well. In figure 8 the total flux is plotted. The sediment flux is in the direction of the arrows; the magnitude of the sediment flux is denoted by the length of the arrows. The fluxes at the entrance are largest (as can be seen from figure 7b). Behind the maximum of the bottom profile, it is seen that the sediment is transported from the crests in the direction of the end of the embayment, but that the lateral diffusion transports it towards the centre of the embayment, where the troughs are found. Hence a net sediment flux acts from crest to trough which results in a negative feedback mechanism and hence in negative growth rates of the bottom perturbations.

Furthermore, note from figures 7(a), 7(b) and 8 that the embayment is split into two parts that do not exchange sediment. There is a region near the entrance of the embayment where sediment is exported towards the sea. Next a location in the embayment is found where sediment is only transported in the lateral direction. Finally in the region close to the landward boundary the sediment is only redistributed. Obviously, away from the entrance of the embayment the dynamics are not influenced by the possible net import or export of sediment from the sea.

Thus we conclude that in order to have morphologic instabilities, a mechanism should be included which causes a decrease (increase) of the tidal flow while moving in shallower (deeper) water. For irrotational flow this is not possible, but it can occur if the bottom friction terms depend on the water depth. In that case smaller depths induce larger decelerations of the tidal flow over the bars and thus provide instability conditions. Physically this means that bottom frictional torques are generated and thus vorticity is produced: the flow will no longer be irrotational. This will be investigated in the next section.

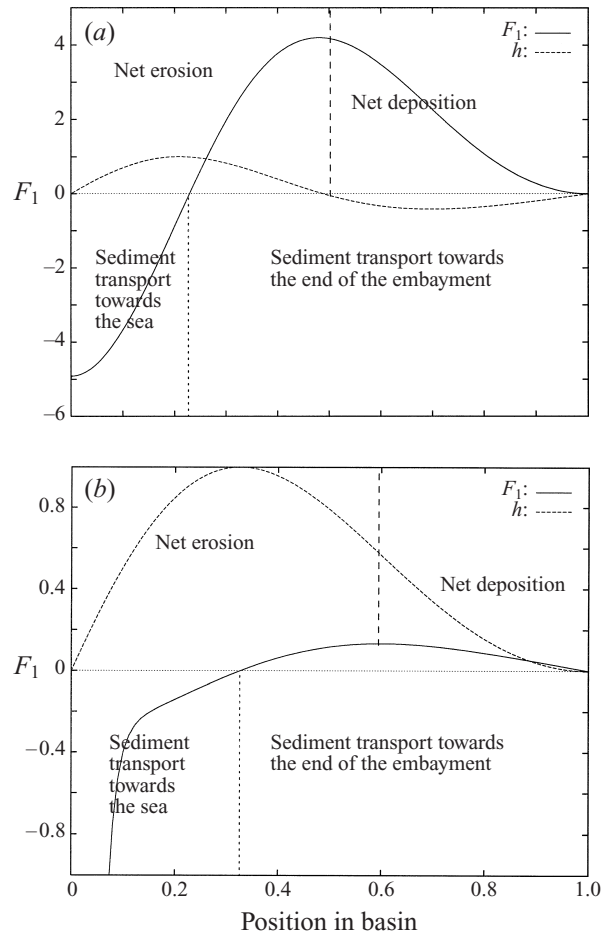


FIGURE 7. Sediment fluxes in the longitudinal direction and bottom profile for (a)  $l_n = 0$  and (b)  $l_n = 60$ , with  $\delta = 0.01$  and  $\lambda = 0$ . Here the first longitudinal mode is chosen.

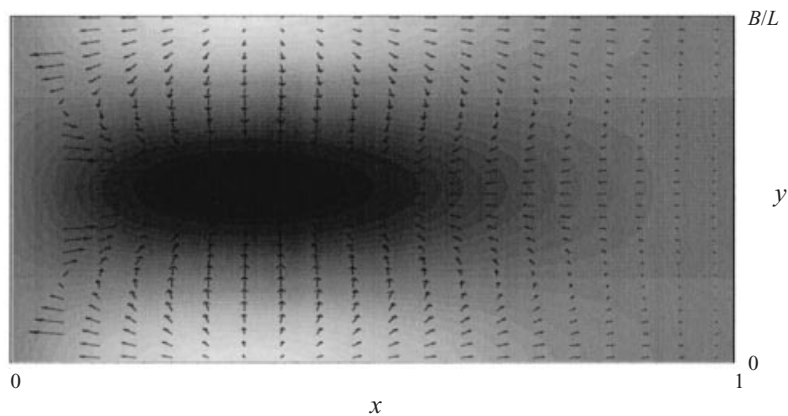


FIGURE 8. Plot of the bottom profile with  $l_n = 60$ ,  $n = 2$ , first longitudinal mode. The crests of the profile are white, the trough is black. The arrows denote the sediment flux. The parameters used were  $\delta = 0.01$ ,  $\lambda = 0$ .

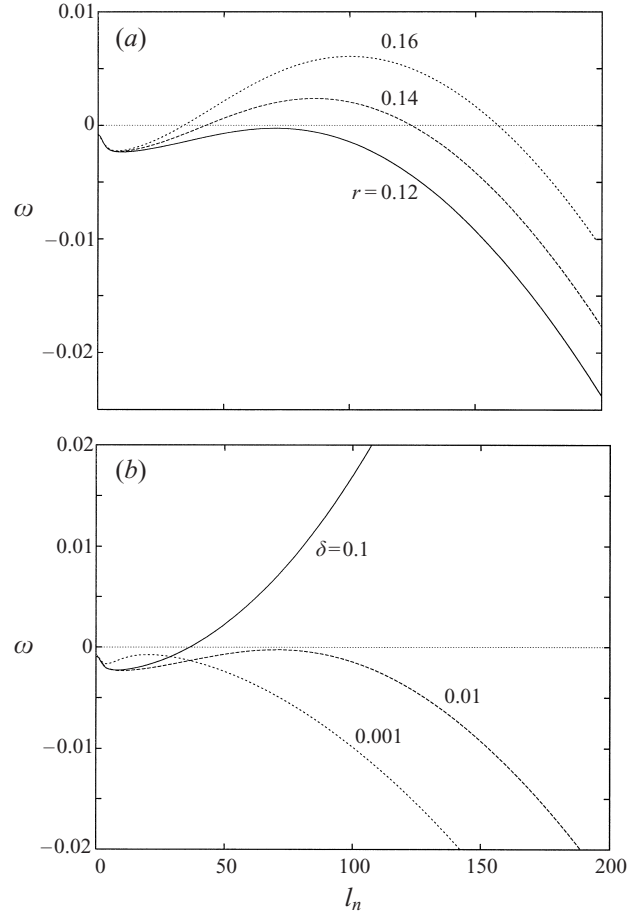


FIGURE 9. The first longitudinal eigenvalue for (a) different values of  $r$  and  $\delta = 0.01$ , and (b) different values of  $\delta$  and  $r = 0.12$ ;  $\eta = 1$  and  $\lambda = 10^{-6}$ .

## 6. Frictional torques

In this section,  $\eta \neq 0$  which implies that the bottom friction terms depend on the water depth. As a consequence, vorticity is not conserved, thus equations (4.9) for  $\{u_n^s, v_n^s\}$  and  $\{u_n^c, v_n^c\}$  are coupled. If the bedload contribution is neglected ( $\lambda = 0$ ), it can be shown (see the Appendix, § A.2) that the basic state becomes unstable with respect to small-scale perturbations (i.e. large values of  $l_n$ ). Therefore, the gravitational effect will not be neglected in the remainder of this section.

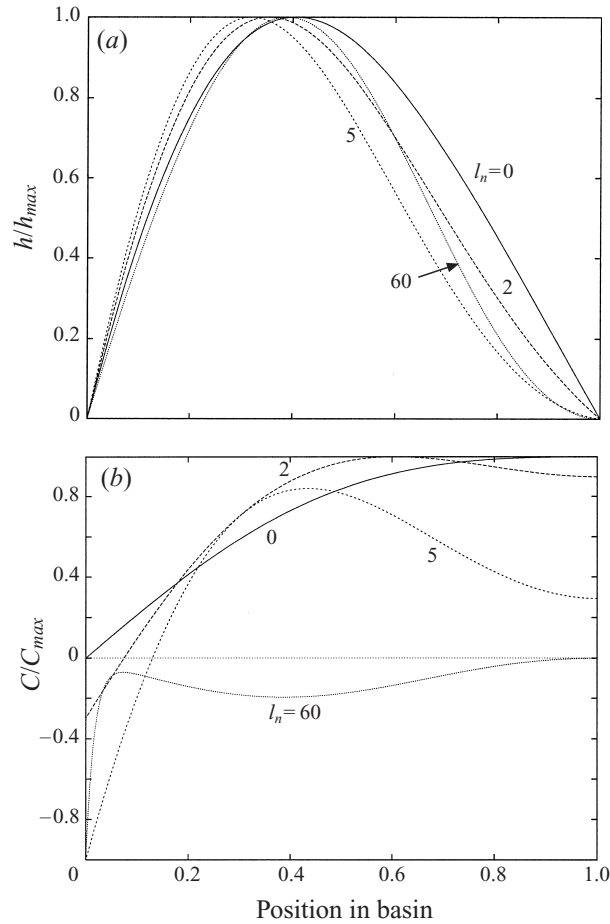
In figure 9(a) the growth rate is shown as a function of the lateral wavenumber  $l_n$  for various values of the friction parameter  $r$ , keeping  $\eta = 1$ ,  $\lambda = 10^{-6}$  and  $\delta = 0.01$  fixed. An important difference with the irrotational flow case of the previous section is that now a positive feedback can exist between the bottom and the water motion. As can be seen in figure 9(b), which shows the growth rate for  $r = 0.12$  and different values of  $\delta$ , the instability mechanism becomes more efficient with increasing  $\delta$ , i.e. smaller grain sizes.

In figure 10(a) bottom profiles are shown for different wavenumbers  $l_n$  and  $\delta = 0.01$ ,  $r = 0.14$ ,  $\eta = 1.0$  and  $\lambda = 10^{-6}$ . In figure 10(b) the concentration profiles and in

---

Wavenumber $l_n$	$h_{max}$	$C_{max}$	$u_{max}^s$	$u_{max}^c$	$v_{max}^s$	$v_{max}^c$
0	1	2.29	2.29	0	0	0
2	1	1.26	1.26	0.04	1.85	0.63
5	1	0.58	0.58	0.09	1.30	0.64
60	1	0.07	0.07	0.13	0.18	0.00

---

TABLE 3. Maxima of the various physical quantities for different values of  $l_n$  (frictional model).FIGURE 10. Plot of first longitudinal eigenmode for (a) the bottom profiles and (b) concentrations for  $\delta = 0.01$ ,  $\lambda = 10^{-6}$ ,  $\eta = 1$ ,  $r = 0.14$  and different  $l_n$ .

figures 11 and 12 the velocity profiles are plotted. In table 3 the maxima of the relevant physical quantities are given.

Similarities with the results in § 5.1 are that the maximum in the concentration profile shifts towards the seaward end of the embayment if the wavenumber  $l_n$  is increased and that a diffusive boundary layer develops near this location. Of course, differences can be noted as well. The most important ones are that in the frictionless case the components of the velocity field  $u_n^c$  and  $v_n^c$  that describe the  $\cos t$ -behaviour on the short time scale do not result in morphodynamic changes (see § 5), whereas

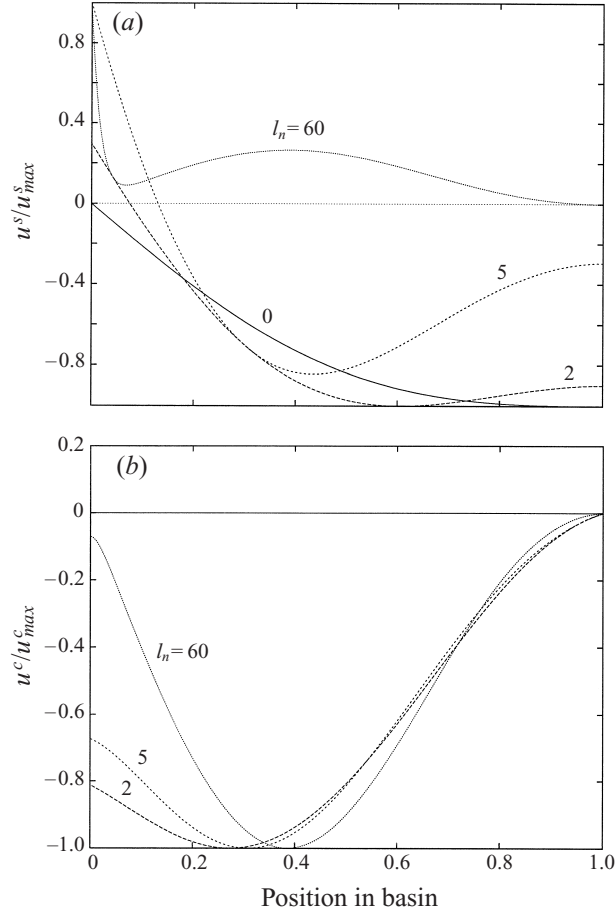


FIGURE 11. Plot of the first eigenmode of the components (a)  $u_n^s$  and (b)  $u_n^c$  of the velocity in the longitudinal direction for  $\delta = 0.01$ ,  $\lambda = 10^{-6}$ ,  $\eta = 1$ , and  $r = 0.14$  and different  $l_n$ .

in the frictional case they have a contribution in the morphodynamic changes by interaction with the components  $u_n^s$  and  $v_n^s$ . Furthermore, the concentration profile can have a local minimum where the bottom profile attains a maximum (see the  $l_n = 60$  mode). Owing to the phase shift in time between the velocity components, the location of the maxima and minima of the concentration can differ from those of the bottom perturbations, thereby allowing instability.

In figure 13 the neutral stability curve  $\omega = 0$  of the first eigenmode in the longitudinal direction is plotted as a function of the lateral wavenumber  $l_n$  and the friction parameter  $r$ ; the other parameter values are  $\delta = 0.01$ ,  $\eta = 1$  and  $\lambda = 10^{-6}$ . It appears that other longitudinal modes have smaller growth rates. The figure indicates that below a critical value  $r_{cr} \approx 0.123$ , all perturbations are damped, while for  $r_{cr}$  some of the perturbations have a positive growth rate.

Of course, by increasing  $\lambda$  (larger bedload contribution) or by decreasing  $\delta$  (smaller horizontal mixing or larger grain sizes) these modes can be stabilized. To understand the instability, we consider the mode with  $\eta = 1$ ,  $r = 0.14$ ,  $\delta = 0.01$ ,  $\lambda = 10^{-6}$  and  $l_n = 60$  with  $n = 2$  (see for example table 1; for the Frisian inlet system, the  $n = 2$  lateral mode would be the first unstable mode). For this mode, the bottom profile and

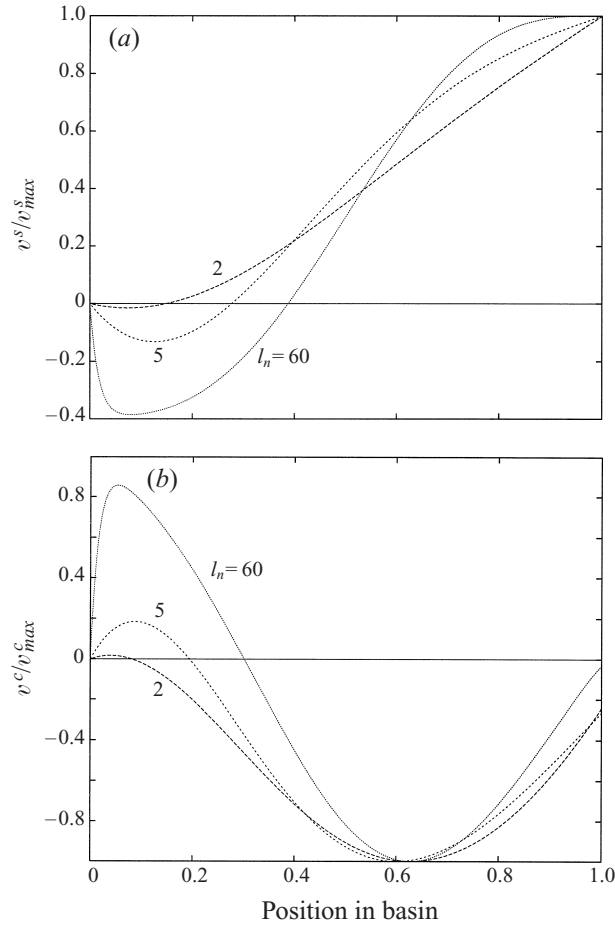


FIGURE 12. Plot of the first eigenmode of the components (a)  $v_n^s$  and (b)  $v_n^c$  of the velocity in the lateral direction for  $\delta = 0.01$ ,  $\lambda = 10^{-6}$ ,  $\eta = 1$ ,  $r = 0.14$  for different  $l_n$ .

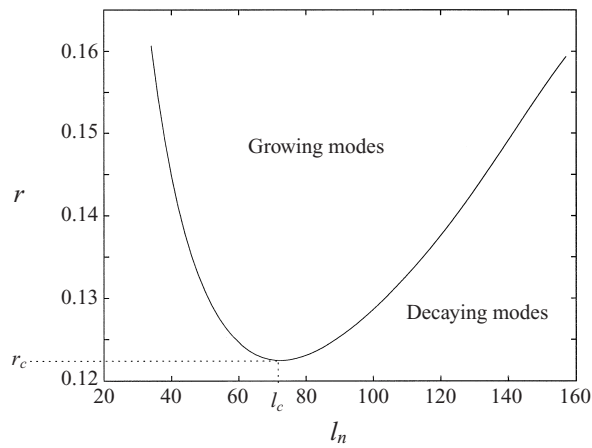


FIGURE 13. Neutral stability curve obtained by varying the friction parameter  $r$ . The parameters used were  $\delta = 0.01$ ,  $\lambda = 10^{-6}$  and  $\eta = 1$ .

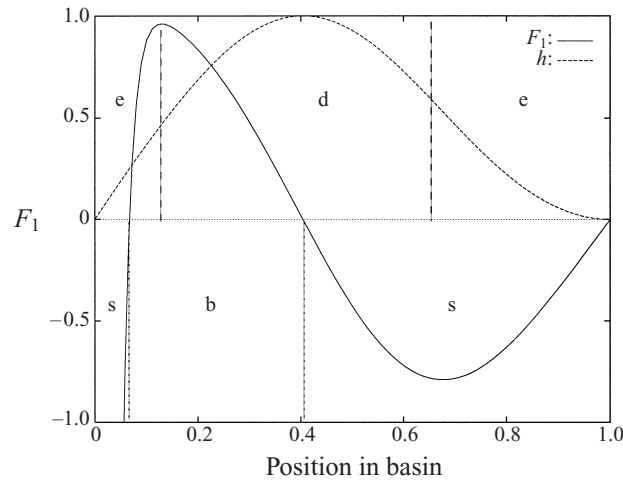


FIGURE 14. Longitudinal sediment flux and bottom profile for  $l_n = 60$ ,  $n = 2$ . The parameters used were  $\delta = 0.01$ ,  $\lambda = 10^{-6}$ ,  $r = 0.14$  and  $\eta = 1$ . In this figure *s* stands for sediment moved towards the open sea, *b* for sediment moved into the embayment, *e* for regions in the embayment where net erosion occurs and *d* those regions where net deposition is found.

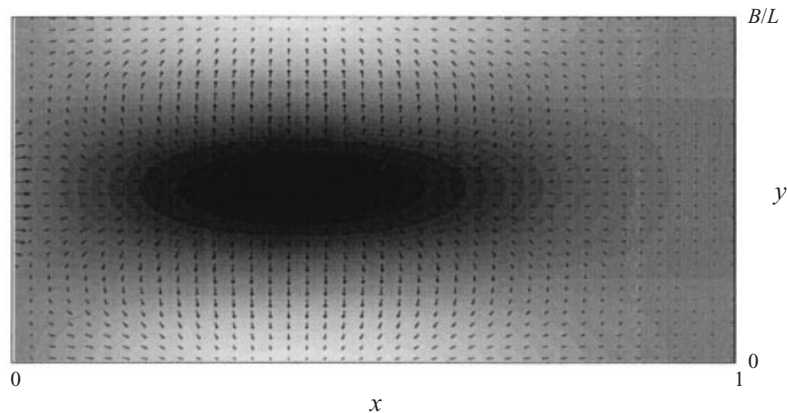


FIGURE 15. Plot of the bottom profile with  $l_n = 60$ ,  $n = 2$ . The crests of the profile are white, the trough is black. The arrows denote the sediment flux. The parameters used were  $\delta = 0.01$ ,  $\lambda = 10^{-6}$ ,  $r = 0.14$  and  $\eta = 1$ .

the sediment flux in the longitudinal direction are plotted in figure 14. In figure 15 the spatial distribution of sediment flux due to concentration gradients is plotted. The crucial difference with the results of the irrotational model (see figures 7 and 8) is that in this case the crest of the perturbation coincides with a convergence of sediment. Physically this is due to the production of vorticity by bottom frictional torques. They cause the longitudinal velocity (and thereby the concentration) to become slightly smaller above the shoals and larger in the channels. This results in a net diffusive sediment flux from the troughs towards the crests. Furthermore, it appears that three regions can be distinguished in the embayment. The first is close to the sea where large fluxes of sediment are entering and leaving without penetrating far into the embayment. The second region is observed a little farther into the embayment,

where the sediment moves from the seaward side towards the crests. The last region is observed near the end of the embayment where the sediment moves from the landward side towards the crests.

## 7. Discussion and conclusions

In this paper, we showed that the formation of channels and shoals in tidal embayments with a finite width-to-length ratio can be explained as a positive feedback mechanism between the tidal flow and the bottom. The water motion was described by the shallow water equations, neglecting Coriolis terms. The embayments were considered to be short compared to the tidal wavelength and driven by an externally prescribed tide. It was assumed that only the diffusion of sediment in suspension and bedslope effects could result in net sediment transport. Since the tidal time scale is much shorter than the morphodynamic time scale, the method of averaging was applied to separately describe the dynamics of the water motion and the bottom. Owing to these assumptions, a comparison can only be made with a small number of embayments, for example with the Frisian Inlet. However, the assumptions were only made to keep the analysis transparent and to keep the computational effort to a minimum, since our main interest was to get a better understanding of the basic mechanism that results in instabilities in tidal embayments.

The assumptions underlying the present model can be relaxed and in that case more realistic results are to be expected. However, it is worth mentioning that already this simple system has an equilibrium state in which the bed shear stress is spatially uniform, in accordance with observations (Friedrichs 1995). Furthermore, the model predicts a net import of sediment after a partial closure, so it captures much of the necessary physics.

It appears that a necessary condition for instability is the presence of bottom frictional torques which cause the tidal velocity to decrease above the shoals and to increase in the channels. If the effect of the frictional torques is stronger than the continuity effect (which causes the water to slow down in the channel and to speed up over the shoals) the bottom perturbations can grow. This explains the presence of a critical friction parameter  $r_c$  in figure 13, below which all modes exponentially decay. Moreover, it explains why no instabilities were found in case of an irrotational flow: it is essential that friction depends on the water depth.

A necessary condition for the damping of short-scale modes is the introduction of a bedslope term in the total load sediment flux. This causes the system to become selective, i.e. a critical lateral wavenumber is found at which the constantly sloping bottom becomes first unstable. The wavenumber depends (among other things) on the length  $L$  and width  $B$  of the embayment. If the length is kept fixed, a critical width  $B$  is found for which the equilibrium profile becomes unstable for the first time. The selected wavenumber depends on the value of the parameters  $r$  (which describes the strength of the friction),  $\delta$  (related to the grain size) and  $\lambda$  (which measures the strength of the bedslope term).

The critical mode for the parameters of the Frisian inlet system ( $l_c \sim 60$ ) gives encouraging results since it predicts that the constantly sloping bottom becomes unstable and channels are formed. The critical friction coefficient ( $r_c \sim 0.125$ ) appears to be quite small: realistic values for  $r$  are 0.5–0.8. This suggests that in a natural embayment many modes will be unstable and after the initial stage they will interact. As a consequence the long-term behaviour of the bedforms will be complicated.

It appears that the structure of the instabilities found is such that three distinct

regions can be identified in the embayment. Between these regions, no exchange of sediment is found. Therefore, the large fluxes of sediment near the entrance of the embayment (and hence the boundary conditions at the open end) do not play a very important role in the behaviour of the perturbation inside the embayment and hence do not influence the instability mechanism. Exchange of sediment between these different regions will probably occur if advective contributions or nonlinear effects are taken into account.

At this point, only real eigenvalues are found. This means that bedforms do not migrate. Probably the introduction of advective terms in both the shallow water equations and in the concentration equation will result in moving bedforms. The perturbations resemble in some sense the observed channel–shoal systems in tidal embayments: but in order to understand their long-term behaviour a fully nonlinear model is necessary. This is presently under investigation and some indicative results are discussed in Schuttelaars (1997, 1998).

This research was supported by NWO-grant no. NLS 61-261 and by the EU-sponsored Marine Science and Technology Programme (MAST-III), under contract no. MAS3-CT95-0002 (PACE project). Furthermore, we thank A. van Harten and A. Doelman for their comments on earlier versions of this paper.

## **Appendix. Asymptotic analysis for large mode numbers**

### *A.1. The frictionless case*

In this Appendix, it will be shown that for large values of the parameter  $l_n = n\pi L/B$  the eigenvalues of the corresponding eigenmodes tend to go to zero if no bedload transport is incorporated in our model. Large values of  $l_n$  mean  $l_n^2 \delta^2 \gg 1$ . First, we combine the continuity equation (4.2a) and vorticity equation (4.2b) and introduce the expansion (4.7) to find the following differential equation for  $u$  (note that subscripts  $n$  in the state variables are dropped):

$$\left[ \frac{1}{1-x} [(1-x)u]_x \right] + l_n^2 u = \left( \frac{h_x}{1-x} \right)_x. \quad (\text{A } 1)$$

Near  $x = 0$  and  $x = 1$  the full equations are necessary to describe  $u$ . Away from the boundaries, we use  $l_n^2 \gg 1$  and hence the first term on the left-hand side of (A 1) is much smaller than the second term. Thus  $u$  can be approximated by

$$u = \frac{1}{l_n^2} \left( \frac{h_x}{1-x} \right)_x. \quad (\text{A } 2)$$

Furthermore, it follows from both the numerical results and the boundary condition (4.6b) that  $h \rightarrow 0$  as  $x \rightarrow 1$ . Note that our approximation becomes better as  $l_n \rightarrow \infty$ .

The concentration equation is given by

$$C + u = \delta^2 (C_{xx} - l_n^2 C).$$

As an approximation for the concentration for  $l_n^2 \delta^2 \gg 1$ , away from  $x = 0$  and  $x = 1$  where boundary layer corrections must be calculated, we can use

$$C \approx -\frac{u}{\delta^2 l_n^4}. \quad (\text{A } 3)$$

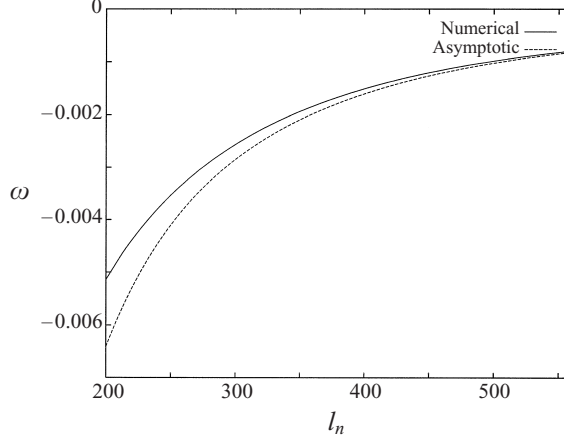


FIGURE 16. Comparison of numerically found eigenvalues and asymptotic eigenvalues for  $\delta = 0.01$ .

Substituting these results in the bottom evolution equation we obtain

$$h_t = C + u = \left( \frac{1}{l_n^2} - \frac{1}{\delta^2 l_n^4} \right) \left( \frac{h_x}{(1-x)} \right)_x. \quad (\text{A } 4)$$

If we use as boundary conditions that near  $x = 1$  the sediment flux  $-C_x$  is zero and  $h/(1-x)$  must be finite and that near  $x = 0$  the bottom perturbation  $h = 0$ , this equation can be solved in terms of Bessel functions (see Schuttelaars & de Swart 1996). As a first approximation the eigenvalues must satisfy (since  $\delta^2 l_n^2 \gg 1$ )

$$J_{2/3} \left( \frac{2}{3} l_n (-\omega)^{1/2} \right) = 0$$

with  $J_{2/3}$  the first-order Bessel function of index  $2/3$ . If we denote the first zero of  $J_{2/3}(\xi)$  by  $\rho$ , we find that the growth rate  $\omega$  is given by

$$\omega = -\frac{9\rho^2}{4l_n^2}. \quad (\text{A } 5)$$

Since  $\rho$  is finite and  $l_n \rightarrow \infty$ , it is clear that  $\omega \rightarrow 0$  as  $l_n \rightarrow \infty$ . Furthermore, we have checked this relation for the first eigenvalue and the numerical results. The results are shown in figure 16. From (A 5) it is seen that  $\omega$  is to leading-order independent of  $\delta$ .

Using the asymptotic equation for  $h$ , it is clear that if the slope term from the bedload transport contribution is retained, this term will always become the largest contribution for  $l_n \gg 1$ . Indeed, if

$$\frac{1}{l_n^2} \ll \lambda l_n^2$$

the bottom evolution equation reduces to a simple diffusion equation due to the bedload contribution. This equation has the appropriate behaviour for large  $l_n$ , namely that the fast oscillating perturbations are damped.

#### A.2. Introducing friction

If friction is introduced, the vorticity equation (4.2b) becomes, after the substitution of the expansions (4.7),

$$iv_x + il_n u = r [(1 + \eta x)] v_x - l_n \left[ -\frac{r\eta}{2i} h + r(1 + \eta x) u \right] \quad (\text{A } 6)$$

Here it is convenient not to split  $u$  and  $v$  in terms proportional to  $\sin t$  and  $\cos t$  but leave them complex. Thus  $u \sim e^{it}$ ,  $v \sim e^{it}$  and  $h$  is real. Outside the boundary layers, we see that for  $l_n \gg 1$  to leading order

$$u = \frac{\eta r}{2i} \frac{1}{i + r[1 + \eta(1 - z)]} h$$

and, using the concentration equation (4.10),

$$C = -\frac{1}{a\mu l_n^2} \text{Re}(u).$$

If  $l_n \gg 1$  then  $\text{Re}(u) \gg C$ . Hence the bottom evolution equation becomes

$$h_\tau = \text{Re}(u) + \dots$$

To illustrate that positive growth rates can be found when friction is included, we first consider  $\eta \ll 1$  and write  $h_\tau = \omega h$ . It then follows that

$$\omega \approx \frac{\eta r^2}{1 + r^2}. \quad (\text{A } 7)$$

If  $\eta$  is small a better approximation has to be made. However, it is clear from the role of  $\eta$  that if  $\eta$  increases, the instability mechanism becomes stronger and hence for large  $l_n$  the eigenmodes become more unstable. Thus for  $\eta \ll 1$ , the growth rate tends to a constant for  $l_n \gg 1$ . This means that very fast oscillating modes are unstable unless  $\lambda \neq 0$ . Of course, this analysis does not deal with all aspects of the model. However it has been verified that both the order of magnitude and the sign of the eigenvalues are given correctly by the above analysis. If  $\lambda \neq 0$ , the bottom evolution equation will become diffusively dominated for  $l_n \gg 1$  and will be dominated by the bedslope terms (see § A.1) and hence the fast oscillating modes will be damped.

#### REFERENCES

- ABRAMOWITZ, M. & STEGUN, I. A. 1965 *Handbook of Mathematical Functions*. Dover.
- AUBREY, D. G. 1990 Interdisciplinary estuarine research: a challenge for the future. In *Residual Currents and Long Term Transport* (ed. R. T. Cheng), pp. 7–14. Springer.
- CSANADY, G. T. 1982 *Circulation in the Coastal Ocean*. Reidel.
- DRONKERS, J. 1986 Tidal asymmetry and estuarine morphology. *Neth. J. Res.* **20**, 117–131.
- DYER, K. R. 1986 *Coastal and Estuarine Sediment Dynamics*. John Wiley & Sons.
- DYER, K. R. & SOULSBY, R. L. 1988 Sand transport on the continental shelf. *Ann. Rev. Fluid Mech.* **20**, 295–324.
- EHLERS, J. 1988 *The Morphodynamics of the Wadden Sea*. Balkema.
- FALQUÉS, A., MONTOTO, A. & IRANZO, V. 1996 Bed-flow instability of the longshore current. *Cont. Shelf Res.* **15**, 1927–1964.
- FREDSOE, J. & DEIGAARD, R. 1992 *Mechanics of Coastal Sediment Transport*. World Scientific.
- FRIEDRICHS, C. T. 1995 Stability shear stress and equilibrium cross-sectional geometry of sheltered tidal channels. *J. Coast. Res.* **11**, 1062–1074.
- FRIEDRICHS, C. T. & AUBREY, D. G. 1994 Tidal propagation in strongly convergent channels. *J. Geophys. Res.* **99**, 3321–3336.
- JONG, K. DE 1998 Tidally averaged transport models. PhD thesis, Delft University of Technology, The Netherlands.
- KROL, M. 1991 On a Galerkin-averaging method for weakly nonlinear wave equations. *Math. Appl. Sci.* **11**, 649–664.
- LORENTZ, H. A. 1922 Het in rekening brengen van den weerstand bij schommelende vloeistofbewegingen. *De Ingenieur* p. 695.

- MCBRIDE, R., BYRNES, M. & HILAND, M. 1995 Geomorphic response-type model for barrier coastlines: a regional perspective. *Mar. Geol.* **126**, 143–159.
- OOST, A. P. 1995 Dynamics and sedimentary development of the Dutch wadden sea with emphasis on the Frisian Inlet. PhD thesis, Utrecht University.
- PARKER, B. B. (Ed.) 1991 *Tidal Hydrodynamics*. John Wiley & Sons.
- RIJN, L. C. VAN 1993 *Principles of Sediment Transport in Rivers, Estuaries and Coastal Seas*. Amsterdam: Aqua Publ.
- RIDDERINKHOF, H. & ZIMMERMAN, J. T. F. 1992 Chaotic stirring in a tidal system. *Science* **258**, 1107–1111.
- SANDERS, J. A. & VERHULST, F. 1985 *Averaging Methods in Nonlinear Dynamical Systems*. Springer.
- SCHIELEN, R., DOELMAN, A. & SWART, H. E. DE 1993 On the nonlinear dynamics of free bars in straight channels. *J. Fluid Mech.* **252**, 325–356.
- SCHUTTELAARS, H. M. 1997 Evolution and stability analysis of bottom patterns in tidal embayments. PhD thesis, University of Utrecht, The Netherlands.
- SCHUTTELAARS, H. M. 1998 Nonlinear, long term equilibrium profiles in a short tidal embayment. In *Physics of Estuaries and Coastal Seas* (ed. J. Dronkers & M. Scheffers), pp. 337–343. PECS 1996 Balkema.
- SCHUTTELAARS, H. M. & SWART, H. E. DE 1996 An idealized long-term morphodynamic model of a tidal embayment. *Eur. J. Mech. B/Fluids*, **15**, 55–80.
- SEMINARA, G. & TUBINO, M. 1998 On the formation of estuarine free bars. In *Physics of Estuaries and Coastal Seas* (ed. J. Dronkers & M. Scheffers), pp. 345–353. PECS 96 Balkema.
- SPEER, P. E. & AUBREY, D. G. 1985 A study of nonlinear tidal propagation in shallow inlet/estuarine systems. Part 2: Theory. *Est. Coastal Shelf Sci.* **21**, 207–224.
- TALMON, A. M., MIERLO, M. C. L. M. VAN & STRUIKSMA, N. 1995 Laboratory measurements of the direction of sediment transport on transverse alluvial bed slopes. *J. Hydr. Res.* **33**, 495–517.
- VAN DONGEREN, A. R. & VRIEND, H. J. DE 1994 A model of morphological behaviour of tidal basins. *Coastal Eng.* **22**, 287–310.
- VREUGDENHIL 1994 *Numerical Methods for Shallow Water Flow*. Kluwer.
- VRIEND, H. DE & RIBBERINK, J. 1996 Mathematical modelling of meso-tidal barrier island coasts. Part ii: Process-based simulation models. In *Advances in Coastal and Ocean Engineering* (ed. P.-F. Liu), pp. 151–197. World Scientific.
- VRIEND, H. J. DE 1996 Mathematical modelling of meso-tidal barrier island coasts. Part i: Empirical and semi-empirical models. In *Advances in Coastal and Ocean Engineering* (ed. P.-F. Liu), pp. 115–149. World Scientific.
- WANG, Z. B., LOUTERS, T. & VRIEND, H. J. DE 1992 A morphodynamic model for a tidal inlet. In *Computing Modelling in Ocean Engineering '91 – Proc. Second Intl Conf., Barcelona, 30 September – 4 October 1991* (ed. A. Arcilla & Others), pp. 235–245. Balkema.
- WANG, Z., LOUTERS, T. & VRIEND, H. DE 1995 Morphodynamic modelling for a tidal inlet in the wadden sea. *Mar. Geol.* **126**, 289–300.
- ZIMMERMAN, J. T. F. 1982 On the Lorentz linearization of a quadratically damped forced oscillator. *Phys. Lett.* **89A**, 123–124.
- ZIMMERMAN, J. T. F. 1992 On the Lorentz linearization of a nonlinearly damped tidal Helmholtz oscillator. *Proc. Kon. Ned. Akad. v. Wetensch.* **95** 127–145.